Noname manuscript No.
(will be inserted by the editor)

Normal Integration – Part I: A Survey

Yvain Quéau · Jean-Denis Durou · Jean-François Aujol

the date of receipt and acceptance should be inserted later

Abstract The need for efficient normal integration methods is driven by several computer vision tasks such as shape-from-shading, photometric stereo, deflectometry, etc. Our work is divided into two papers. In the present paper entitled *Part I: A Survey*, we select the most important properties that one may expect from a normal integration method, based on a thorough study of two pioneering works by Horn and Brooks [27] and by Frankot and Chellappa [19]. Apart from accuracy, an integration method should at least be fast and robust to a noisy normal field. In addition, it should be able to handle both several types of boundary condition, including the case of a free boundary, and a domain of reconstruction of any shape i.e., which is not necessarily rectangular. It is also much appreciated that a minimum number of parameters have to be tuned, or even no parameter at all. Finally, it should preserve the depth discontinuities. In view of this analysis, we review most of the existing methods, and conclude that none of them satisfies all of the required properties. In the second paper entitled *Part II: New Insights*, we focus on the problem of normal integration in the presence of depth discontinuities, a problem which occurs as soon as there are occlusions.

Keywords 3D-reconstruction, integration, normal field, gradient field.

Y. Quéau
Technical University Munich, Germany
E-mail: yvain.queau@tum.de

J.-D. Durou
IRIT, Université de Toulouse, France

J.-F. Aujol
IMB, Université de Bordeaux, France
Institut Universitaire de France

1 Introduction

Computing the 3D-shape of a surface from a set of normals is a classical problem of 3D-reconstruction called *normal integration*. This problem is well-posed, except that a constant of integration has to be fixed, but its resolution is not as straightforward as it could appear, even in the case of a dense discrete normal field i.e., when the normal to a surface is known at every pixel of an image. One may well be surprised that such a simple problem has given rise to such a large number of papers. This is probably due to the fact that, like many computer vision problems, it simultaneously meets several requirements. Of course, a method of integration is expected to be accurate, fast, and robust re noisy data or outliers, but we will see that several other criteria are important as well.

The present contribution to the resolution of normal integration is organized in two parts. In the present paper entitled *Part I: A Survey*, a thorough study of two pioneering works is done: a paper by Horn and Brooks based on variational calculus [27]; another one by Frankot and Chellappa resorting to Fourier analysis [19]. This preliminary study allows us to select six criteria apart from accuracy, through which we intend to *qualitatively* evaluate the main existing normal integration methods. Our survey is summarized in Table 1. Knowing that, in light of the selected criteria, no existing method is completely satisfactory, this preliminary study impels us to suggest several new methods of integration, which will be found in a second paper entitled *Part II: New Insights*.

The organization of the present paper is the following. We derive the basic equations of normal integration in Section 2. Horn and Brooks' and Frankot and Chellappa's methods are reviewed in Section 3. This al-

lows us, in Section 4, to select several properties that are required by any normal integration method, and to comment the most relevant related works. In Section 5, we conclude that a completely satisfactory method of integration is still lacking, which justifies the need for new methods.

2 Basic Equations of Normal Integration

Suppose that, in each point $\mathbf{x}' = [u, v]^\top$ of the image of a surface, the unit-length outgoing normal $\mathbf{n}(u, v) = [n_1(u, v), n_2(u, v), n_3(u, v)]^\top$ is known. Such a function $\mathbf{n}$ constitutes what is called a *normal field*. Integrating a normal field consists in searching for three functions x, y and z (z is usually called the *depth*, or even the *height*) such that the normal to the surface at the object point $\mathbf{x}(u, v) = [x(u, v), y(u, v), z(u, v)]^\top$, which is conjugate to the image point $\mathbf{x}'$, is equal to $\mathbf{n}(u, v)$. In this section, we recall how to rigorously formulate this problem when the projection model is either weak-perspective or perspective. A preliminary version of this study was originally conducted in [16].

We attach a 3D-frame $\mathbf{c}xyz$ to the camera, whose origin $\mathbf{c}$ is located at the optical center and such that the axis $\mathbf{c}z$ coincides with the optical axis (cf. Fig. 1). The camera is focused on a plane π of equation $z = \mathsf{d}$, which is conjugate to the image plane π'. In practice, π' coincides with the focal plane of equation $z = \mathsf{f}$, where f denotes the focal length.

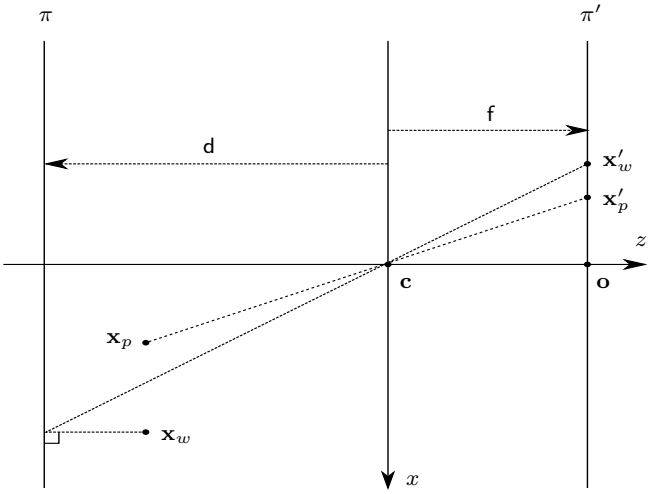

Fig. 1 Orthographic projection: $\mathbf{x}_w$ is conjugate to $\mathbf{x}'_w$. Perspective projection: $\mathbf{x}_p$ is conjugate to $\mathbf{x}'_p$.

2.1 Weak-perspective Projection

Under the assumption of weak-perspective projection (see the points $\mathbf{x}_w$ and $\mathbf{x}'_w$ in Fig. 1), $x(u, v)$ and $y(u, v)$ are worth:

$$\begin{cases} x(u, v) = \dfrac{\mathsf{d}}{\mathsf{f}}\, u \\ y(u, v) = \dfrac{\mathsf{d}}{\mathsf{f}}\, v \end{cases} \tag{1}$$

Let us introduce the image magnification $\mathsf{m} = \mathsf{f}/\mathsf{d}$. The cross product of both partial derivatives $\partial_u \mathbf{x}_w$ and $\partial_v \mathbf{x}_w$ reads (the dependencies in u and v are omitted, for the sake of simplicity):

$$\partial_u \mathbf{x}_w \times \partial_v \mathbf{x}_w = \frac{1}{\mathsf{m}^2} \left[-\mathsf{m}\, \partial_u z, -\mathsf{m}\, \partial_v z, 1\right]^\top \tag{2}$$

This vector being normal to the surface, its cross product by $\mathbf{n}(u, v)$ is null. This gives us the three following equations, which are linear with respect to the two unknowns $\partial_u z$ and $\partial_v z$:

$$\begin{cases} \mathsf{m}\, n_3\, \partial_u z = -n_1 \\ \mathsf{m}\, n_3\, \partial_v z = -n_2 \\ n_2\, \partial_u z - n_1\, \partial_v z = 0 \end{cases} \tag{3}$$

System (3) is non-invertible if the rank of its matrix is less than 2 i.e., if $n_3^2 = n_1\, n_3 = n_2\, n_3 = 0$, which occurs if and only if $n_3 = 0$. This particular case must be considered with attention, since it means that $\mathbf{n}(u, v)$ is parallel to the image plane π'. Under the assumption of weak-perspective projection, an image point satisfies this property if and only if it lies on the *occluding contour*. Thus, even if the normal is easy to determine for the image points which lie on the occluding contour (the normal is parallel to π' and is normal to this contour), z cannot be computed for such points.

Now, let us consider the image points which do not lie on the occluding contour. System (3) is invertible and its resolution easily gives us the following PDE in z:

$$\nabla z = \frac{1}{\mathsf{m}} \left[p, q\right]^\top \tag{4}$$

where the following classical notations are used:

$$\begin{cases} p = -\dfrac{n_1}{n_3} \\ q = -\dfrac{n_2}{n_3} \end{cases} \tag{5}$$

Thus, the problem of integrating a normal field is the same as integrating the gradient of z. The resolution of Eq. (4) is straightforward:

$$z(u, v) = z(u_0, v_0) + \frac{1}{\mathsf{m}} \int_{(r,s)=(u_0,v_0)}^{(u,v)} \left[p(r, s)\, \mathrm{d}r + q(r, s)\, \mathrm{d}s\right] \tag{6}$$

regardless of the integration path between some point (u_0, v_0) and (u, v), as soon as p and q satisfy the *constraint of integrability* $\partial_v p = \partial_u q$ (Schwartz theorem). Otherwise, the integral in Eq. (6) would depend on the integration path. If there is no point (u_0, v_0) where z is known, it follows from Eq. (6) that $z(u, v)$ is computable up to an additive constant. In such a case, the root mean square error (RMSE) in z depends on this constant which is chosen, in the tests, so that the RMSE is minimal.

2.2 Perspective Projection

Under the assumption of perspective projection (see the points $\mathbf{x}_p$ and $\mathbf{x}'_p$ in Fig. 1), $x(u, v)$ and $y(u, v)$ are worth:

$$\begin{cases} x(u,v) = \dfrac{z(u,v)}{\mathsf{f}}\, u \\ y(u,v) = \dfrac{z(u,v)}{\mathsf{f}}\, v \end{cases} \tag{7}$$

The cross product of $\partial_u \mathbf{x}_p$ and $\partial_v \mathbf{x}_p$ is a little more complicated to compute than in the weak-perspective case:

$$\partial_u \mathbf{x}_p \times \partial_v \mathbf{x}_p = \frac{z}{\mathsf{f}^2} \left[-\mathsf{f}\,\partial_u z, -\mathsf{f}\,\partial_v z, z + u\,\partial_u z + v\,\partial_v z\right]^\top \tag{8}$$

Knowing that this vector is parallel to $\mathbf{n}(u, v)$, this gives us the three following equations:

$$\begin{cases} \mathsf{f}\, n_3\, \partial_u z + n_1 \left[z + u\,\partial_u z + v\,\partial_v z\right] = 0 \\ \mathsf{f}\, n_3\, \partial_v z + n_2 \left[z + u\,\partial_u z + v\,\partial_v z\right] = 0 \\ n_2\, \partial_u z - n_1\, \partial_v z = 0 \end{cases} \tag{9}$$

Since this system is homogeneous in z, it is useful to introduce the following change of variable:

$$\tilde{z} = \ln |z| \tag{10}$$

Thus, we obtain three equations which are linear with respect to the two unknowns $\partial_u \tilde{z}$ and $\partial_v \tilde{z}$:

$$\begin{cases} \left[\mathsf{f}\, n_3 + u\, n_1\right] \partial_u \tilde{z} + v\, n_1\, \partial_v \tilde{z} = -n_1 \\ u\, n_2\, \partial_u \tilde{z} + \left[\mathsf{f}\, n_3 + v\, n_2\right] \partial_v \tilde{z} = -n_2 \\ n_2\, \partial_u \tilde{z} - n_1\, \partial_v \tilde{z} = 0 \end{cases} \tag{11}$$

This last system is non-invertible if the rank of its matrix is less than 2, i.e.:

$$\begin{cases} \mathsf{f}\, n_3 \left[u\, n_1 + v\, n_2 + \mathsf{f}\, n_3\right] = 0 \\ -n_1 \left[u\, n_1 + v\, n_2 + \mathsf{f}\, n_3\right] = 0 \\ -n_2 \left[u\, n_1 + v\, n_2 + \mathsf{f}\, n_3\right] = 0 \end{cases} \tag{12}$$

As n_1, n_2 and n_3 cannot simultaneously vanish, because $\mathbf{n}$ is a unit-length vector, System (12) holds if and only if $u\, n_1 + v\, n_2 + \mathsf{f}\, n_3 = 0$. Knowing that $\mathbf{x}'_p - \mathbf{c} = [u, v, \mathsf{f}]^\top$, it happens that $u\, n_1 + v\, n_2 + \mathsf{f}\, n_3 = (\mathbf{x}'_p - \mathbf{c}) \cdot \mathbf{n}$ (Fig. 1). Therefore, as in the weak-perspective case, System (12) holds if and only if the image point $\mathbf{x}'_p$ lies on the occluding contour (which differs from the previous occluding contour, defined under weak-perspective projection).

If we consider the image points which do not lie on the occluding contour, System (11) is invertible and its resolution gives us a PDE in $\tilde{z}$:

$$\nabla \tilde{z} = [\tilde{p}, \tilde{q}]^\top \tag{13}$$

where $\tilde{p}$ and $\tilde{q}$ stand for the following expressions:

$$\begin{cases} \tilde{p} = -\dfrac{n_1}{u\, n_1 + v\, n_2 + \mathsf{f}\, n_3} \\ \tilde{q} = -\dfrac{n_2}{u\, n_1 + v\, n_2 + \mathsf{f}\, n_3} \end{cases} \tag{14}$$

As in the weak-perspective case, the problem of integrating a normal field is that of integrating the gradient of $\tilde{z}$. Solving Eq. (13) is straightforward:

$$\tilde{z}(u, v) = \tilde{z}(u_0, v_0) + \int_{(r,s)=(u_0,v_0)}^{(u,v)} \left[\tilde{p}(r, s)\, \mathrm{d}r + \tilde{q}(r, s)\, \mathrm{d}s\right] \tag{15}$$

From (15) and (10), we deduce:

$$z(u, v) = z(u_0, v_0)\, \exp\left\{ \int_{(r,s)=(u_0,v_0)}^{(u,v)} \left[\tilde{p}(r, s)\, \mathrm{d}r + \tilde{q}(r, s)\, \mathrm{d}s\right] \right\} \tag{16}$$

Once again, Eqs. (15) and (16) hold if and only if $\tilde{p}$ and $\tilde{q}$ satisfy the constraint of integrability $\partial_v \tilde{p} = \partial_u \tilde{q}$ (see Section 2.3).

It follows from Eq. (16) that z can be computed up to a multiplicative constant. Notice also that (14), and therefore (16), require that the focal length f is known, as well as the location of the principal point $\mathbf{o}$, since the coordinates u and v depend on it.

The strict similarity between (4) and (13) shows us that any normal integration method can be extended to the perspective case, provided that the intrinsic parameters of the camera are known[1]. Let us emphasize that this possible extension to perspective projection is *generic* i.e., it is not restricted to a given method of integration. So we can limit ourselves to solve the following equation:

$$\nabla z(u, v) = \mathbf{g}(u, v) \tag{17}$$

where $(z, \mathbf{g}) = (z, \frac{1}{\mathsf{m}} [p, q]^\top)$ in the weak-perspective case, and $(z, \mathbf{g}) = (\tilde{z}, [\tilde{p}, \tilde{q}]^\top)$ in the perspective case. In both cases, we will denote for simplicity:

$$\mathbf{g}(u, v) = \begin{bmatrix} p(u, v) \\ q(u, v) \end{bmatrix} \tag{18}$$

[1] In [51], such an extension is advocated for the integration method designed in [29].

2.3 Integration Using Quadratic Regularization

Knowing that any method of integration can be extended to the perspective case thanks to the change of variable (10), we do not care more whether the projection is weak-perspective or perspective. From now, we just have to solve the generic equation (17).

As already noticed, the solution (6) of Eq. (4), or the solution (15) of Eq. (13), are independent from the integration path if and only if the constraint of integrability $\partial_v p = \partial_u q$, or $\partial_v \tilde{p} = \partial_u \tilde{q}$, are satisfied. A normal field is never rigorously integrable (or *curl-free*) in practice. Apart from using several integration paths and then taking the means of the integrals [12,25,57], the most natural way to deal with the lack of integrability is to consider Eq. (17) as an optimization problem [27]. Using quadratic regularization, this amounts to minimizing the following functional:

$$\mathcal{F}_{L_2}(z) = \iint\limits_{(u,v)\in\Omega} \|\nabla z(u,v) - \mathbf{g}(u,v)\|^2 \,\mathrm{d}u\,\mathrm{d}v \tag{19}$$

where $\Omega \subset \mathbb{R}^2$ denotes the *domain of integration*, and $\mathbf{g} = [p,q]^\top$ is the datum of the problem, which we call the *gradient field*. This functional is strictly convex in ∇z, but it does not admit a unique minimizer z^* since, for any constant $K \in \mathbb{R}$, $\mathcal{F}_{L_2}(z^* + K) = \mathcal{F}_{L_2}(z^*)$.

The minimization of $\mathcal{F}_{L_2}(z)$ requires that the associated Euler-Lagrange equation is satisfied. The calculus of variation provides us with the following:

$$\nabla \mathcal{F}_{L_2}(z) = 0 \quad \Longleftrightarrow \quad -2\,\mathrm{div}\,(\nabla z - \mathbf{g}) = 0 \tag{20}$$

This necessary condition is rewritten as the following *Poisson equation*[2]:

$$\Delta z = \partial_u p + \partial_v q \tag{21}$$

Solving Eq. (21) is not a sufficient condition for minimizing $\mathcal{F}_{L_2}(z)$, but this is the case if z is known on the boundary $\partial\Omega$ of Ω (Dirichlet boundary condition), see [38] and the references therein. In the absence of such boundary condition, the so-called *natural boundary condition*, which is of the Neumann type, must be considered. In the case of $\mathcal{F}_{L_2}(z)$, this boundary condition is written [27]:

$$(\nabla z - \mathbf{g}) \cdot \boldsymbol{\eta} = 0 \tag{22}$$

where $\boldsymbol{\eta}$ is the outer unit-length normal to the boundary $\partial\Omega$ in the image plane.

Solving the same Poisson equation (21), but using different boundary conditions, one could expect that both solutions would coincide on most part of Ω, but this is not true. For a given gradient field $\mathbf{g}$, the choice of a boundary condition, including the natural boundary condition when only $\mathbf{g}$ is known, has a great influence on the 3D-reconstructed shape. This is noted in [27]: "[Eq. (21)] does not uniquely specify a solution without further constraint. In fact, we can add any harmonic function to a solution to obtain a different solution also satisfying" Eq. (21). A *harmonic function* is a solution of the *Laplace equation*:

$$\Delta z = 0 \tag{23}$$

As an example, let us search for the harmonic functions taking the particular form $z(u,v) = z_1(u)\,z_2(v)$. Writing Eq. (23), and knowing that $z(u,v) \neq 0$ implies $z_1(u,v) \neq 0$ and $z_2(u,v) \neq 0$, we obtain:

$$\frac{z_1''(u)}{z_1(u)} = -\frac{z_2''(v)}{z_2(v)} \tag{24}$$

Both sides of Eq. (24) must thus be equal to a common constant $K \in \mathbb{R}$. Two cases may occur, according to the sign of K. For $K = -\omega^2$, $\omega \in \mathbb{R}$:

$$\begin{cases} z_1''(u) + \omega^2\, z_1(u) = 0 \\ z_2''(v) - \omega^2\, z_2(v) = 0 \end{cases} \quad \Longrightarrow \quad \begin{cases} z_1(u) = z_1(0)\, e^{\mathrm{j}\,\omega u} \\ z_2(v) = z_2(0)\, e^{\omega v} \end{cases} \tag{25}$$

where j is such that $\mathrm{j}^2 = -1$. Finally, we obtain:

$$z(u,v) = z(0,0)\, e^{\omega(\mathrm{j}\,u + v)} \tag{26}$$

Note that a real harmonic function defined on $\mathbb{R}^2$ can be considered as the real part or as the imaginary part of a *holomorphic function*. All the functions of the form (26) are indeed holomorphic. Their real and imaginary parts thus provide us with the following two families of harmonic functions:

$$\{\cos(\omega u)\, e^{\omega v}\}_{\omega\in\mathbb{R}} \quad ; \quad \{\sin(\omega u)\, e^{\omega v}\}_{\omega\in\mathbb{R}} \tag{27}$$

Adding to a given solution of the Poisson equation (21) any linear combination of these harmonic functions (there exist many others), we obtain other solutions of the same equation. The way to select the right solution is to carefully manage the boundary. In the case of a free boundary, the variational calculus tells us that minimizing $\mathcal{F}_{L_2}(z)$ requires that Eq. (22) is imposed on the boundary, but we know that the solution is still non-unique, since it is known up to an additive constant. The same conclusion holds true for any Neumann boundary condition. On the other hand, as soon as Ω is bounded, a Dirichlet boundary condition ensures uniqueness of the solution, but not existence.

[2] Similar equations arise in several computer vision problems [3,44,49].

3 Two Pioneering Normal Integration Methods

Before a more exhaustive review, we first make a thorough study of two pioneering normal integration methods which have very different peculiarities. This will allow us to detect the most important properties that one may expect from any method of integration.

3.1 Horn and Brooks' Method

A well-known normal integration method due to Horn and Brooks [27], which we denote by $\mathcal{M}_{\text{HB}}$, attempts to minimize the following discrete approximation of $\mathcal{F}_{L_2}(z)$, where the (u,v) denote the *pixels* of a square 2D-grid:

$$F_{L_2}(\mathbf{z}) = \sum_{(u,v)\in\Omega_1} \left[\frac{z_{u+1,v}-z_{u,v}}{\delta} - \frac{p_{u+1,v}+p_{u,v}}{2}\right]^2 + \sum_{(u,v)\in\Omega_2} \left[\frac{z_{u,v+1}-z_{u,v}}{\delta} - \frac{q_{u,v+1}+q_{u,v}}{2}\right]^2 \tag{28}$$

In (28), δ is the distance between neighbouring pixels (in the following, the scale is chosen so that $\delta = 1$), Ω_1 denotes the set of pixels $(u,v) \in \Omega$ such that $(u+1,v) \in \Omega$, Ω_2 the set of pixels $(u,v) \in \Omega$ such that $(u,v+1) \in \Omega$, and $\mathbf{z}$ the vector $[z_{u,v}]_{(u,v)\in\mathring{\Omega}}$, where $\mathring{\Omega} = \Omega \backslash \partial\Omega$ is the set of pixels $(u,v) \in \Omega$ whose four nearest neighbours are inside Ω. Horn and Brooks suppose that the values $z_{u,v}$, for $(u,v) \in \partial\Omega$, are known. This means that a Dirichlet boundary condition is considered.

For any point $(u,v) \in \mathring{\Omega}$, one gets from (28) and from the characterization $\nabla F_{L_2} = 0$ of an extremum:

$$z_{u+1,v} + z_{u-1,v} + z_{u,v+1} + z_{u,v-1} - 4\, z_{u,v} = \frac{p_{u+1,v} - p_{u-1,v}}{2} + \frac{q_{u,v+1} - q_{u,v-1}}{2} \tag{29}$$

Eqs. (29), for $(u,v) \in \mathring{\Omega}$, form a discrete approximation of the Poisson equation (21), if finite differences to the second order are used to approximate both the Laplacian and the divergence. As stated in [24], other choices can be considered, as long as the orders of the finite differences are consistent. In [27], Eqs. (29) are solved using a Jacobi iteration:

$$z_{u,v}^{k+1} = \frac{z_{u+1,v}^{k} + z_{u-1,v}^{k} + z_{u,v+1}^{k} + z_{u,v-1}^{k}}{4} - \frac{p_{u+1,v} - p_{u-1,v}}{8} - \frac{q_{u,v+1} - q_{u,v-1}}{8} \tag{30}$$

The initialization is not a cause for concern, since $F_{L_2}(\mathbf{z})$ is convex. Moreover, it is standard to show the convergence of this scheme [50], but it converges very slowly if the initialization is far from the solution [16].

3.2 Improvement of Horn and Brooks' Method

Dirichlet boundary conditions are rarely available in practice, but $\mathcal{M}_{\text{HB}}$ can be extended, in order to properly manage any Neumann boundary condition, including the natural boundary condition (22). An improved version of Horn and Brooks' method, originally designed by Durou and Courteille in [16] and denoted by $\mathcal{M}_{\text{DC}}$, considers all the values $z_{u,v}$ as unknowns i.e., even for $(u,v) \in \partial\Omega$. Of course, the equation $\partial F_{L_2}/\partial z_{u,v} = 0$ does not take the form (29) any more, for $(u,v) \in \partial\Omega$. Let us take the example of a pixel $(u,v) \in \partial\Omega$ such that $(u+1,v)$ and $(u,v+1)$ are inside Ω, while $(u-1,v)$ and $(u,v-1)$ are outside Ω (cf. Fig. 2). Then, (29) must be replaced with:

$$z_{u+1,v} + z_{u,v+1} - 2\, z_{u,v} = \frac{p_{u+1,v} + p_{u,v}}{2} + \frac{q_{u,v+1} + q_{u,v}}{2} \tag{31}$$

On the other hand, since $\boldsymbol{\eta} = -\sqrt{2}/2\,[1,1]^\top$ is a plausible outer unit-length normal to the boundary $\partial\Omega$ in this case, the natural boundary condition (22) reads:

$$\partial_u z - p + \partial_v z - q = 0 \tag{32}$$

It is obvious that (31) is a discrete approximation of (32). More generally, it is easily shown that the equation $\partial F_{L_2}/\partial z_{u,v} = 0$, for any $(u,v) \in \partial\Omega$, is the discrete approximation of the natural boundary condition (22).

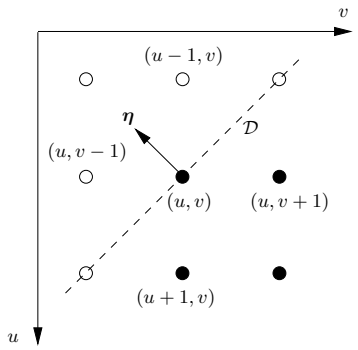

Fig. 2 Only the black pixels are inside Ω. The straight line $\mathcal{D}$ is a plausible approximation of the tangent to $\partial\Omega$ at (u,v).

Therefore, this simple idea suffices to design an improved version $\mathcal{M}_{\text{DC}}$ of $\mathcal{M}_{\text{HB}}$ which does not require any extra knowledge on z, except that z has to be fixed at one point of Ω, because of the additive constant $z(u_0,v_0)$ in (6) or $\tilde{z}(u_0,v_0)$ in (15). However, even if it is recommended to fix $z(u_0,v_0)$ from a computational point of view, in order to avoid a possible drift, the choice of this constant has no importance at all. We choose it so that the RMSE is minimal, as soon as

the ground truth is available[3]. Otherwise, it is chosen so that the mean of z is equal to zero.

Let us test $\mathcal{M}_{\text{HB}}$ and $\mathcal{M}_{\text{DC}}$ on the surface $\mathcal{S}_{\text{vase}}$ shown in Fig. 3-a, which models a half-vase lying on a flat ground. To this end, we discretize the *analytically computed* gradient field of $\mathcal{S}_{\text{vase}}$ on a regular grid of size 312×312, and we first use as domain of integration Ω_{vase} the set of points which lie on the vase. We suppose that the only data are Ω_{vase} and the gradient of $\mathcal{S}_{\text{vase}}$. Since the method $\mathcal{M}_{\text{HB}}$ requires the knowledge of the depth on the boundary, we fix $z = 0$ on $\partial\Omega_{\text{vase}}$. Knowing that this is clearly false at the top and at the bottom of the vase, the result will probably be degraded. The 3D-reconstructions obtained at convergence, using $\mathcal{M}_{\text{HB}}$ (with the boundary condition $z = 0$) and $\mathcal{M}_{\text{DC}}$ (with the natural boundary condition), are shown in Figs. 3-b and 3-c. The second result is qualitatively much better, since the top and the bottom of the vase are not flattened. This is confirmed by the RMSE. We conclude that $\mathcal{M}_{\text{DC}}$ improves Horn and Brooks' original method $\mathcal{M}_{\text{HB}}$ a lot, when the depth is neither known nor equal to 0 on the boundary.

On the other hand, it is well-known that quadratic regularization is not well-adapted to discontinuities. Let us now test $\mathcal{M}_{\text{DC}}$ on the whole gradient field of $\mathcal{S}_{\text{vase}}$ i.e., using the whole grid of size 312×312 as domain of integration. The 3D-reconstruction at convergence is shown in Fig. 3-d. It is not satisfactory, since the discontinuities are not preserved, which is numerically confirmed by the RMSE. We know that removing the flat ground from the domain of integration suffices to reach a better result (cf. Fig. 3-c), since this eliminates any depth discontinuity from the domain of integration. However, this requires a preliminary segmentation of the scene, which is known to be a hard task, and also requires that the integration can be carried out on a *non-rectangular domain of integration*.

3.3 Frankot and Chellappa's Method

A more general approach to overcome the possible non-integrability of the gradient field $\mathbf{g} = [p, q]^\top$ is to first define a set $\mathcal{I}$ of integrable vector fields i.e., of vector fields of the form ∇z, and then compute the projection $\nabla\bar{z}$ of $\mathbf{g}$ on $\mathcal{I}$ i.e., the vector field $\nabla\bar{z}$ of $\mathcal{I}$ the closest to $\mathbf{g}$, according to some norm. Afterwards, the (approximate) solution of Eq. (17) is easily obtained using Eq. (6) or Eq. (16), since $\nabla\bar{z}$ is integrable. Nevertheless, the boundary conditions can be complicated to manage, because $\mathcal{I}$ depends on which boundary condition is imposed (including the case of the natural boundary condition). It is noticed in [2] that minimizing the functional $\mathcal{F}_{L_2}(z)$ amounts to following this general approach, in the case where $\mathcal{I}$ contains all integrable vector fields and the Euclidean norm is used.

The most cited normal integration method, due to Frankot and Chellappa [19], follows this approach in the case where the Fourier basis is considered. Let us use the standard definition of the Fourier transform:

$$\hat{f}(\omega_u, \omega_v) = \iint_{(u,v)\in\mathbb{R}^2} f(u,v)\, e^{-\mathrm{j}\,\omega_u\, u}\, e^{-\mathrm{j}\,\omega_v\, v}\, \mathrm{d}u\, \mathrm{d}v \tag{33}$$

where the *pulsations* (ω_u, ω_v) are real. Computing the Fourier transforms of both sides of Eq. (21), we obtain:

$$-(\omega_u^2 + \omega_v^2)\, \hat{z}(\omega_u, \omega_v) = \mathrm{j}\,\omega_u\, \hat{p}(\omega_u, \omega_v) + \mathrm{j}\,\omega_v\, \hat{q}(\omega_u, \omega_v) \tag{34}$$

For any (ω_u, ω_v) such that $\omega_u^2 + \omega_v^2 \neq 0$, Eq. (34) gives us the following expression of $\hat{z}(\omega_u, \omega_v)$:

$$\hat{z}(\omega_u, \omega_v) = \frac{\omega_u\, \hat{p}(\omega_u, \omega_v) + \omega_v\, \hat{q}(\omega_u, \omega_v)}{\mathrm{j}\,(\omega_u^2 + \omega_v^2)} \tag{35}$$

Indeed, computing the inverse Fourier transform of the expression (35) of $\hat{z}(\omega_u, \omega_v)$ provides us a solution of Eq. (21). This method of integration [19], denoted by $\mathcal{M}_{\text{FC}}$, is very fast thanks to the FFT algorithm.

The Fourier transform can be confusing: with the alternative definition using *frequencies* instead of pulsations, a 2π factor would arise in the denominator of the right member of Eq. (35). In [39], it is written that the accuracy of Frankot and Chellappa's method relies on a good input scale: we guess that this scale is $(2\pi)^{-1}$.

Since Eq. (35) is not defined if $(\omega_u, \omega_v) = (0, 0)$, Frankot and Chellappa assert that it "simply means that we cannot recover the average value of z without some additional information". This is true but incomplete, because $\mathcal{M}_{\text{FC}}$ provides the solution of Eq. (21) *up to the addition of a harmonic function* over Ω. Saracchini et al. note in [48] that "the homogeneous version of Eq. (21) is satisfied by an arbitrary linear function of position $z(u, v) = a\,u + b\,v + c$, which when added to any solution of Eq. (21) will yield infinitely many additional solutions". Affine functions are harmonic indeed, but we know from Section 2.3 that many other harmonic functions also exist.

Applying $\mathcal{M}_{\text{FC}}$ to the gradient field of $\mathcal{S}_{\text{vase}}$ would give us a similar result to that of Fig. 3-d, but much faster, if the domain of integration is equal to the whole grid. However, such a result as that of Fig. 3-c could not be reached, since $\mathcal{M}_{\text{FC}}$ is not designed to manage a non-rectangular domain Ω.

[3] The same procedure is used by Klette and Schlüns in [35]: "The reconstructed height values are shifted in the range of the original surface using LSE optimization".

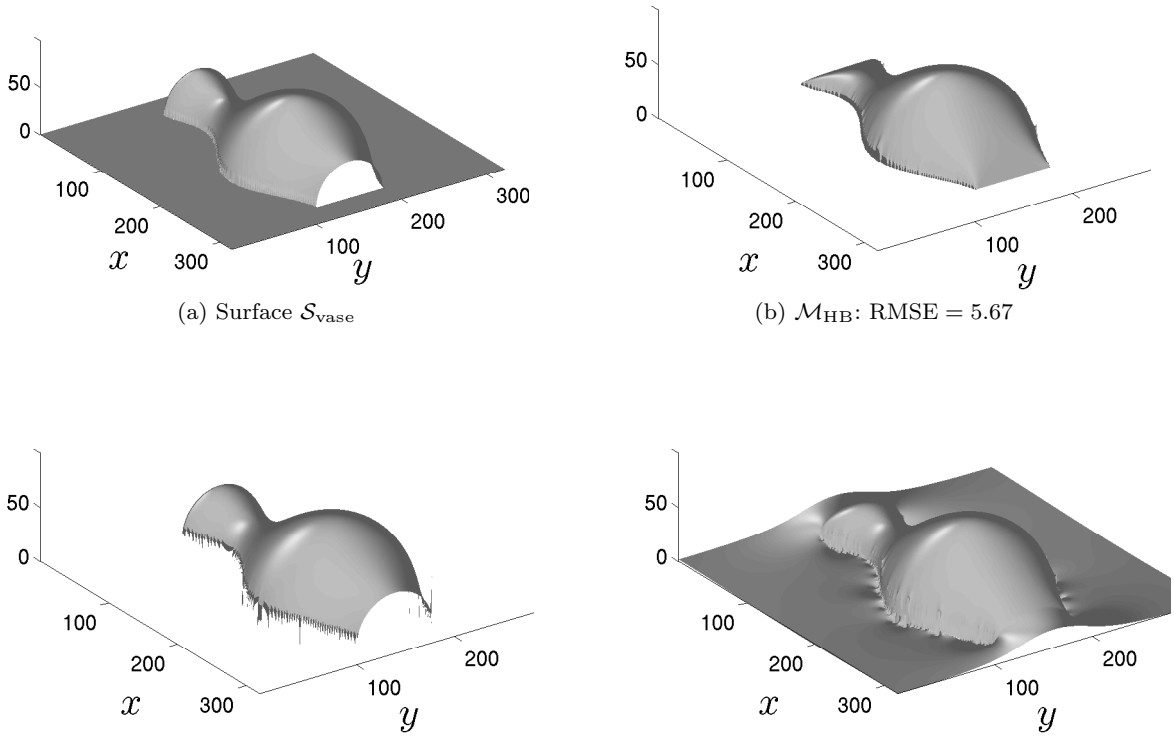

(a) Surface $\mathcal{S}_{\text{vase}}$ (b) $\mathcal{M}_{\text{HB}}$: RMSE = 5.67

(c) $\mathcal{M}_{\text{DC}}$: RMSE = 0.93 (d) $\mathcal{M}_{\text{DC}}$: RMSE = 4.51

Fig. 3 (a) Surface $\mathcal{S}_{\text{vase}}$. 3D-reconstructions obtained by integration of the gradient field of $\mathcal{S}_{\text{vase}}$, when the domain of integration Ω_{vase} contains only the pixels lying on the vase, applying: (b) 100 iterations of $\mathcal{M}_{\text{HB}}$; (c) 100 iterations of $\mathcal{M}_{\text{DC}}$. (d) 3D-reconstruction obtained by integration of the gradient field of $\mathcal{S}_{\text{vase}}$, if the domain of integration is equal to the whole grid, applying 100 iterations of $\mathcal{M}_{\text{DC}}$. In order to limit the bias, it is important both to use the natural boundary condition and to appropriately handle depth discontinuities.

On the other hand, $\mathcal{M}_{\text{FC}}$ works well if and only if the surface to be reconstructed is periodic. This clearly appears in the example of Fig. 4: the gradient field of a face (cf. Fig. 4-a), estimated via photometric stereo [54], is integrated using $\mathcal{M}_{\text{FC}}$, which results in the 3D-reconstruction shown in Fig. 4-b. Since the real shape is non-periodic, this method much distorts the 3D-reconstruction. This failure of $\mathcal{M}_{\text{FC}}$ was first exhibited by Harker and O'Leary in [22], who show on some examples that the solution provided by $\mathcal{M}_{\text{FC}}$ is not always a minimizer of the functional $\mathcal{F}_{L_2}(z)$. They moreover explain: "The fact that the solution [of Frankot and Chellappa] is constrained to be periodic leads to a systematic bias in the solution" (this periodicity is clearly visible on the recovered shape of Fig. 4-b). Harker and O'Leary also conclude that "any approach based on the Euler-Lagrange equation is only valid for a few special cases". As we will see, this assertion is exaggerated.

3.4 Improvements of Frankot and Chellappa's Method

A first improvement of $\mathcal{M}_{\text{FC}}$ suggested by Simchony, Chellappa and Shao in [49] consists in solving the discrete approximation (29) of the Poisson equation using the discrete Fourier transform, instead of discretizing the solution (35) of the Poisson equation (21).

Consider a rectangular domain $\Omega = [0, d_u]\times[0, d_v] \subset \mathbb{R}^2$, and choose a lattice of $m \times n$ equally spaced points $(u\frac{d_u}{m}, v\frac{d_v}{n})$, $u \in [0, m-1]$, $v \in [0, n-1]$. Let us denote by $f_{u,v}$ the value of a function $f : \Omega \to \mathbb{R}$ at $(u\frac{d_u}{m}, v\frac{d_v}{n})$. The standard definition of the *discrete* Fourier transform of f is as follows, for $k \in [0, m-1]$ and $l \in [0, n-1]$:

$$\hat{f}_{k,l} = \sum_{u=0}^{m-1} \sum_{v=0}^{n-1} f_{u,v}\, e^{-\mathrm{j}2\pi \frac{uk}{m}}\, e^{-\mathrm{j}2\pi \frac{vl}{n}} \tag{36}$$

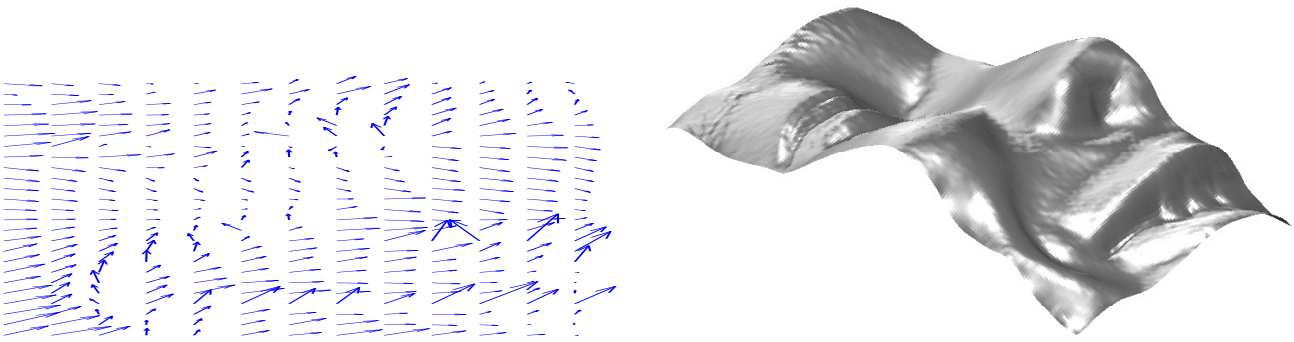

(a) (b)

Fig. 4 (a) Gradient field estimated via photometric stereo. (b) Integration using a periodic boundary condition [19]. The depth is exactly the same on the left and right edges, i.e. on the cheek and on the nose, which much distorts the 3D-reconstruction.

The inverse transform of (36) reads:

$$f_{u,v} = \frac{1}{mn} \sum_{k=0}^{m-1} \sum_{l=0}^{n-1} \hat{f}_{k,l}\, e^{+\mathrm{j}2\pi \frac{ku}{m}}\, e^{+\mathrm{j}2\pi \frac{lv}{n}} \tag{37}$$

Replacing any term in (29) by its inverse discrete Fourier transform of the form (37), and knowing that the Fourier family is a basis, we obtain:

$$\begin{aligned} &2\left[\cos\left(2\pi\tfrac{k}{m}\right) + \cos\left(2\pi\tfrac{l}{n}\right) - 2\right] \hat{z}_{k,l} \\ &\quad = \mathrm{j}\left[\sin\left(2\pi\tfrac{k}{m}\right)\, \hat{p}_{k,l} + \sin\left(2\pi\tfrac{l}{n}\right)\, \hat{q}_{k,l}\right] \end{aligned} \tag{38}$$

Eq. (38) does not provide us any information on $\hat{z}_{0,0}$. On the other hand, as soon as $(k,l) \neq (0,0)$, Eq. (38) gives us the expression of $\hat{z}_{k,l}$:

$$\hat{z}_{k,l} = \frac{\sin\left(2\pi\tfrac{k}{m}\right)\, \hat{p}_{k,l} + \sin\left(2\pi\tfrac{l}{n}\right)\, \hat{q}_{k,l}}{4\mathrm{j}\left[\sin^2\left(\pi\tfrac{k}{m}\right) + \sin^2\left(\pi\tfrac{l}{n}\right)\right]} \tag{39}$$

which is rewritten by Simchony et al. as follows:

$$\hat{z}_{k,l} = \frac{\sin\left(2\pi\tfrac{k}{m}\right)\, \hat{p}_{k,l} + \sin\left(2\pi\tfrac{l}{n}\right)\, \hat{q}_{k,l}}{\mathrm{j}\left[\frac{\sin^2\left(2\pi\frac{k}{m}\right)}{\cos^2\left(\pi\frac{k}{m}\right)} + \frac{\sin^2\left(2\pi\frac{l}{n}\right)}{\cos^2\left(\pi\frac{l}{n}\right)}\right]} \tag{40}$$

Comparing (33) and (36) shows us that ω_u corresponds to $2\pi\frac{k}{m}$ and ω_v to $2\pi\frac{l}{n}$. Using these correspondences, we would expect to be able to identify (35) and (40). This is true if $\sin\left(2\pi\frac{k}{m}\right)$ and $\sin\left(2\pi\frac{l}{n}\right)$ tend toward 0, and $\cos^2\left(\pi\frac{k}{m}\right)$ and $\cos^2\left(\pi\frac{l}{n}\right)$ tend toward 1, which occurs if k takes either the first values or the last values inside $[0, m-1]$, and the same for l inside $[0, n-1]$, which is interpreted by Simchony et al. as follows: "At low frequencies our result is similar to the result obtained in [19]. At high frequencies we attenuate the corresponding coefficients since our discrete operator has a low-pass filter response [...] the surface z obtained in [19] may suffer from high frequency oscillations". Actually, the low values of k and l correspond to the lowest values of ω_u and ω_v inside $\mathbb{R}^+$, and the high values of k and l may be interpreted as the lowest absolute values of ω_u and ω_v inside $\mathbb{R}^-$.

On the other hand, using the inverse discrete Fourier transform (37), the solution of (29) which follows from (39) will be periodic in u with period d_u, and in v with period d_v. This means that $z_{m,v} = z_{0,v}$, for $v \in [1,n]$, and $z_{u,n} = z_{u,0}$, for $u \in [1,m]$. The discrete Fourier transform is therefore appropriate only for problems which satisfy periodic boundary conditions.

Other improvements of $\mathcal{M}_{\mathrm{FC}}$ due to Simchony et al. are to suggest that using the discrete sine transform or the discrete cosine transform would be more appropriate if the problem involves, respectively, Dirichlet or Neumann boundary conditions.

Dirichlet Boundary Condition Any function that is expressed in the form of an inverse discrete sine transform:

$$f_{u,v} = \frac{4}{mn} \sum_{k=1}^{m-1} \sum_{l=1}^{n-1} \bar{f}_{k,l} \sin\left(\pi\frac{ku}{m}\right) \sin\left(\pi\frac{lv}{n}\right) \tag{41}$$

satisfies the homogeneous Dirichlet condition $f_{u,v} = 0$ on the boundary of the discrete domain $\Omega = [0,m] \times [0,n]$ i.e., for $u = 0$, $u = m$, $v = 0$, and $v = n$.

To solve (29) on a rectangular domain Ω with the homogeneous Dirichlet condition $z_{u,v} = 0$ on $\partial\Omega$, we can therefore write $z_{u,v}$ as in (41). This is still possible for a non-homogeneous Dirichlet boundary condition:

$$z_{u,v} = b^D_{u,v} \quad \text{for } (u,v) \in \partial\Omega \tag{42}$$

A first solution would be to solve a pair of problems. Suppose, on the one hand, that $z^0_{u,v}$ is a solution of the

equations (29) written in the form (41), and on the other hand, that $h_{u,v}$ is a harmonic function on Ω (see Section 2.3) that satisfies the boundary condition (42). Then, $z^0_{u,v} + h_{u,v}$ is a solution of the equations (29) that satisfies this boundary condition.

But it is much easier to replace $z_{u,v}$ by $z_{u,v} - b^D_{u,v}$ on $\partial\Omega$. This trick has two advantages. First, it does not change $z_{u,v}$ on $\mathring{\Omega}$ i.e., where it is unknown. Second, the Dirichlet boundary condition satisfied by this new definition of $z_{u,v}$ is homogeneous, so we can actually write $z_{u,v}$ on $\mathring{\Omega}$ under the form (41). In practice, we just have to change the second members of the equations (29) for the points of Ω which are adjacent to the boundary $\partial\Omega$. For all $v \in [1, n-1]$ and all $u \in [1, m-1]$:

$$\begin{cases} g^D_{1,v} = \dfrac{p_{2,v} - p_{0,v}}{2} + \dfrac{q_{1,v+1} - q_{1,v-1}}{2} - b^D_{0,v} \\ g^D_{m-1,v} = \dfrac{p_{m,v} - p_{m-2,v}}{2} + \dfrac{q_{m-1,v+1} - q_{m-1,v-1}}{2} - b^D_{m,v} \\ g^D_{u,1} = \dfrac{p_{u+1,1} - p_{u-1,1}}{2} + \dfrac{q_{u,2} - q_{u,0}}{2} - b^D_{u,0} \\ g^D_{u,n-1} = \dfrac{p_{u+1,n-1} - p_{u-1,n-1}}{2} + \dfrac{q_{u,n} - q_{u,n-2}}{2} - b^D_{u,n} \end{cases} \tag{43}$$

Using the fact that the products of sine functions in (41) form a free family, we get from (29) and (41):

$$\bar{z}_{k,l} = -\frac{\bar{g}^D_{k,l}}{4\left(\sin^2\frac{\pi k}{2m} + \sin^2\frac{\pi l}{2n}\right)},\ (k,l) \in [1, m-1]\times[1, n-1] \tag{44}$$

From (44), we easily deduce $z_{u,v}$ using the inverse discrete sine transform (41).

Neumann Boundary Condition The reasoning is similar in the case of a Neumann boundary condition. Any function that is expressed in the form of an inverse discrete cosine transform[4]:

$$f_{u,v} = \frac{4}{mn}\sum_{k=0}^{m}\sum_{l=0}^{n}\bar{\bar{f}}_{k,l}\cos\left(\pi\frac{ku}{m}\right)\cos\left(\pi\frac{lv}{n}\right) \tag{45}$$

satisfies the homogeneous Neumann boundary condition $\nabla f_{u,v} \cdot \boldsymbol{\eta}_{u,v} = 0$ on $\partial\Omega$, as soon as the following discrete approximation of the gradient is used:

$$\nabla f_{u,v} \approx \frac{1}{2}\begin{bmatrix} f_{u+1,v} - f_{u-1,v} \\ f_{u,v+1} - f_{u,v-1} \end{bmatrix} \tag{46}$$

To solve Eqs. (29) on a rectangular domain Ω with the homogeneous Neumann condition $\nabla z_{u,v} \cdot \boldsymbol{\eta}_{u,v} = 0$ on $\partial\Omega$, we can therefore write $z_{u,v}$ as in (45). This is still possible for a non-homogeneous Neumann boundary condition:

$$\nabla z_{u,v} \cdot \boldsymbol{\eta}_{u,v} = b^N_{u,v} \quad \text{for } (u,v) \in \partial\Omega \tag{47}$$

by changing the definition of $z_{u,v}$ on the outer boundary of Ω[5], which has the same two advantages as previously. First, this does not change $z_{u,v}$ on Ω i.e., where it is unknown. Second, the Neumann boundary condition satisfied by this new definition of $z_{u,v}$ is homogeneous, so we can actually write $z_{u,v}$ on Ω under the form (45). In practice, we just have to change the second members of the equations (29) for the points of $\partial\Omega$. For all $v \in [1, n-1]$ and all $u \in [1, m-1]$:

$$\begin{cases} g^N_{0,v} = p_{1,v} - p_{0,v} + \dfrac{q_{0,v+1} - q_{0,v-1}}{2} + 2\,b^N_{0,v} \\ g^N_{m,v} = p_{m,v} - p_{m-1,v} + \dfrac{q_{m,v+1} - q_{m,v-1}}{2} + 2\,b^N_{m,v} \\ g^N_{u,0} = \dfrac{p_{u+1,0} - p_{u-1,0}}{2} + q_{u,1} - q_{u,0} + 2\,b^N_{u,0} \\ g^N_{u,n} = \dfrac{p_{u+1,n} - p_{u-1,n}}{2} + q_{u,n} - q_{u,n-1} + 2\,b^N_{u,n} \end{cases} \tag{48}$$

Moreover, in the four corners of $\partial\Omega$:

$$\begin{cases} g^N_{0,0} = p_{1,0} - p_{0,0} + q_{0,1} - q_{0,0} + 2\sqrt{2}\,b^N_{0,0} \\ g^N_{0,n} = p_{1,n} - p_{0,n} + q_{0,n} - q_{0,n-1} + 2\sqrt{2}\,b^N_{0,n} \\ g^N_{m,0} = p_{m,0} - p_{m-1,0} + q_{m,1} - q_{m,0} + 2\sqrt{2}\,b^N_{m,0} \\ g^N_{m,n} = p_{m,n} - p_{m-1,n} + q_{m,n} - q_{m,n-1} + 2\sqrt{2}\,b^N_{m,n} \end{cases} \tag{49}$$

Knowing that the products of cosine functions in (45) form a free family, we get from (29) and (45):

$$\bar{\bar{z}}_{k,l} = -\frac{\bar{\bar{g}}^N_{k,l}}{4\left(\sin^2\frac{\pi k}{2m} + \sin^2\frac{\pi l}{2n}\right)}, \tag{50}$$

$\forall (k,l) \in [0,m]\times[0,n]$, except $(k,l) = (0,0)$ or $(k,l) = (m,n)$. Indeed, we cannot determine the coefficients $\bar{\bar{z}}_{0,0}$ and $\bar{\bar{z}}_{m,n}$, which simply means that the solution of the Poisson equation using a Neumann boundary condition (as, for instance, the natural boundary condition) is computable up to an additive constant, because the terms which correspond to the coefficients $\bar{\bar{f}}_{0,0}$ and $\bar{\bar{f}}_{m,n}$ in the double sum of (45) do not depend on (u,v). Keeping this point in mind, we easily deduce $z_{u,v}$ from (50) using the inverse discrete cosine transform (45).

Accordingly, the method $\mathcal{M}_{\text{SCS}}$ designed by Simchony, Chellappa and Shao in [49] works well even if the surface to be reconstructed is non-periodic (cf. Fig. 5-b). Knowing moreover that it is as fast as $\mathcal{M}_{\text{FC}}$, we conclude that $\mathcal{M}_{\text{SCS}}$ improves Frankot and Chellappa's original method a lot. Let us however note that the

[4] Note that, in the definitions of the three inverse discrete transforms (37), (41) and (45), the sums on k and l are done on three different pairs of intervals.

[5] This is a bit more complicated than in the previous case, since the outgoing unit-length normal $\boldsymbol{\eta}_{u,v}$ can have eight different orientations on $\partial\Omega$.

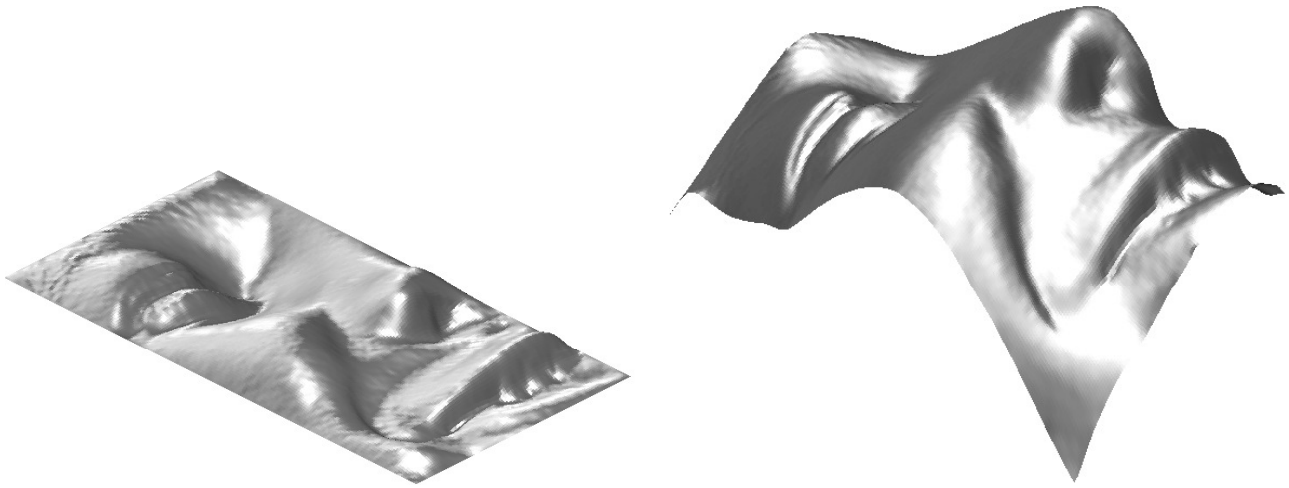

(a) (b)

Fig. 5 (a) Integration of the gradient field of Fig. 4-a using the homogeneous Dirichlet boundary condition $z = 0$: since this is clearly false, the 3D-reconstruction is much distorted. (b) Integration using the (Neumann) natural boundary condition [49]. The natural boundary condition provides much more realistic results.

resolution of the discrete Poisson equation we just described in the case of a Dirichlet or Neumann boundary condition does not exactly match the method $\mathcal{M}_{\text{SCS}}$ described in [49], but is rather intended to be pedagogic.

On the other hand, the useful property of the solutions (41) and (45) i.e., they satisfy a homogeneous Dirichlet or Neumann boundary condition, is obviously valid only if the domain of integration Ω is rectangular. This trick is hence not useable for any other form of domain Ω. It is claimed in [49] that *embedding techniques* can extend $\mathcal{M}_{\text{SCS}}$ to non-rectangular domains, but this is not really proved. As a consequence, such a result as that of Fig. 3-c could not be reached applying $\mathcal{M}_{\text{SCS}}$ to the gradient field of $\mathcal{S}_{\text{vase}}$: the result would be the same as that of Fig. 3-d.

4 Main Normal Integration Methods

4.1 A List of Expected Properties

This may appear as a truism, but a basic requirement of 3D-reconstruction is *accuracy*. Anyway, the evaluation/comparison of 3D-reconstruction methods is a difficult challenge. On the one hand, it may happen that some methods require more data than the others, which makes the evaluation/comparison biased in some sense. On the other hand, it usually happens that the choice of the benchmark has a great influence on the final ranking. Finally, it is a hard task to implement a method just from its description, which gives in practice a substantial advantage to the designers of a ranking process, whatever their methodology, in the case when they also promote their own method. In Section 4.3, we will review the main existing normal integration methods. However, in accordance with these remarks, we do not intend to evaluate their accuracy. We will instead quote their main features.

In view of the detailed reviews of the methods of Horn and Brooks and of Frankot and Chellappa (see Section 3), we may expect, apart from accuracy, five other properties from any normal integration method:

- $\mathcal{P}_{\text{Fast}}$: The desired method should be as *fast* as possible.
- $\mathcal{P}_{\text{Robust}}$: It should be *robust* to a noisy normal field. If the normal field is estimated through photometric stereo, we suppose that the images are corrupted by an additive Gaussian noise, as recommended in [42]: "in previous work on photometric stereo, noise is [wrongly] added to the gradient of the height function rather than camera images".
- $\mathcal{P}_{\text{FreeB}}$: The method should be able to handle a *free boundary*. Accordingly, each method aimed at solving the Poisson equation (21) should be able to solve the natural boundary condition (29) in the same time.
- $\mathcal{P}_{\text{Disc}}$: The method should preserve the *depth discontinuities*. This property could allow us to use photometric stereo on a whole image, without segmenting the scene into different parts without discontinuity.
- $\mathcal{P}_{\text{NoRect}}$: The method should be able to work on a *non-rectangular* domain. This happens when photometric stereo is applied to an object with back-

ground. This property could partly remedy a method which would not satisfy $\mathcal{P}_{\text{Disc}}$, knowing that segmentation is usually easier to manage than preserving the depth discontinuities.

An additional property would also be much appreciated:

- $\mathcal{P}_{\text{NoPar}}$: The method should have *no parameter* to tune (only the *critical* parameters are involved here). In practice, tuning more than one parameter means that an expert of the method is needed. One parameter is often considered as acceptable, but no parameter is even better.

4.2 Integration and Integrability

Among the required properties, we did not *explicitly* quote the ability of a method to deal with non-integrable normal fields, but this is *implicitly* expected through $\mathcal{P}_{\text{Robust}}$ and $\mathcal{P}_{\text{Disc}}$. In other words, the two sources of non-integrability that we consider are noise and depth discontinuities. A normal field estimated using shape-from-shading could be very far from being integrable, because of the ill-posedness of this technique, to such a point that integrability is sometimes used to disambiguate the problem [19,27]. Also the *uncalibrated* photometric stereo problem is ill-posed, and is systematically disambiguated imposing integrability [60]. However, we are over all interested in *calibrated* photometric stereo with $n \geq 3$ images, which is well-posed without resorting to integrability. An error in the intensity of one light source is enough to cause a bias [29], and outliers may appear in shadow regions [46], thus providing normal fields that can be highly non-integrable, but we argue that such defects do not have to be compensated by the integration method itself. In other words, we suppose that the only outliers of the normal field we want to integrate are located on depth discontinuities.

In order to know whether a normal integration method satisfies $\mathcal{P}_{\text{Disc}}$, a shape like $\mathcal{S}_{\text{vase}}$ (cf. Fig. 3-a) is well indicated, but a practical mistake must be avoided, which is not obvious. A discrete approximation of the *integrability term* $\iint_{(u,v)\in\Omega}[\partial_v p(u,v) - \partial_u q(u,v)]^2 \,\mathrm{d}u\,\mathrm{d}v$, which is used in [27] to measure the departure of a gradient field $[p,q]^\top$ from being integrable, is as follows:

$$E_{\text{int}} = \sum_{(u,v)\in\Omega_3} \left[\frac{p_{u,v+1} - p_{u,v}}{\delta} - \frac{q_{u+1,v} - q_{u,v}}{\delta} \right]^2 \tag{51}$$

where Ω_3 denotes the set of pixels $(u,v) \in \Omega$ such that $(u, v+1)$ and $(u+1, v)$ are inside Ω. Let us suppose in addition that the discrete values $p_{u,v}$ and $q_{u,v}$ are *numerically approximated* using the following finite differences:

$$\begin{cases} p_{u,v} = \dfrac{z_{u+1,v} - z_{u,v}}{\delta} \\ q_{u,v} = \dfrac{z_{u,v+1} - z_{u,v}}{\delta} \end{cases} \tag{52}$$

Reporting the expressions (52) of $p_{u,v}$ and $q_{u,v}$ in (51), this always implies $E_{\text{int}} = 0$. Using such a numerically approximated gradient field is thus biased, since it is integrable even in the presence of discontinuities[6], whereas the *analytically computed* gradient field of $\mathcal{S}_{\text{vase}}$ is such that $E_{\text{int}} = 390$.

4.3 Most Representative Normal Integration Methods

The problem of normal integration is sometimes considered as solved, because its mathematical formulation is well established (see Section 2), but we will see that none of the existing methods simultaneously satisfies all the required properties. In the first survey paper on normal integration [35], Klette and Schlüns concluded that "there is a remarkable deficiency of literature about integration techniques, at least in computer vision". Many contributions have appeared afterwards, as well as several surveys [40,46,48], but a detailed review is still missing.

The way to cope with a possible non-integrable normal field was seen as a property of primary importance in the first papers on normal integration. The most obvious way to solve the problem amounts to use different paths in the integral of Eq. (6) and to average the different values. Apart from this approach, which has given rise to several heuristics [12,25,57], we propose to separate the main existing normal integration methods into two classes, depending on whether they care about discontinuities or not.

4.3.1 Methods which do not care about Discontinuities

According to the discussion conducted in Section 2.3, the most natural way to overcome non-integrability is to solve the Poisson equation (21). This approach has given rise to the method $\mathcal{M}_{\text{HB}}$ (see Section 3.1), pioneered by Ikeuchi in [31] and then detailed by Horn and Brooks in [27], which has been the source of inspiration of several subsequent works. The method $\mathcal{M}_{\text{HB}}$ satisfies the property $\mathcal{P}_{\text{Robust}}$ (much better than the heuristics cited above), as well as $\mathcal{P}_{\text{NoPar}}$ (there is no parameter) and $\mathcal{P}_{\text{NoRect}}$, but not $\mathcal{P}_{\text{FreeB}}$. Another drawback of

[6] This problem is also noted by Saracchini et al. in [48]: "Note that taking finite differences of the reference height map will not yield adequate test data".

$\mathcal{M}_{\text{HB}}$ is that it does not satisfy $\mathcal{P}_{\text{Fast}}$, since it uses a Jacobi iteration to solve a large linear system whose size is equal to the number of pixels inside $\mathring{\Omega} = \Omega \backslash \partial\Omega$. Unsurprisingly, $\mathcal{P}_{\text{Disc}}$ is not satisfied by $\mathcal{M}_{\text{HB}}$, since this method does not care about discontinuities.

Frankot and Chellappa address shape-from-shading using a method which "also can be used as an integrator" [19]. The gradient field is projected on a set $\mathcal{I}$ of integrable vector fields ∇z. In practice, the set of functions z is spanned by the Fourier basis. The method $\mathcal{M}_{\text{FC}}$ (see Section 3.3) not only satisfies $\mathcal{P}_{\text{Robust}}$ and $\mathcal{P}_{\text{NoPar}}$, but also $\mathcal{P}_{\text{Fast}}$, since it is non-iterative and, thanks to the FFT algorithm, much faster than $\mathcal{M}_{\text{HB}}$. On the other hand, the domain of integration is implicitly supposed to be rectangular, even if the following is claimed: "The Fourier expansion could be formulated on a finite lattice instead of a periodic lattice. The mathematics are somewhat more complicated [...] and more careful attention could then be paid to boundary conditions". Hence, $\mathcal{P}_{\text{NoRect}}$ is not really satisfied, not more than $\mathcal{P}_{\text{Disc}}$. Finally, $\mathcal{P}_{\text{FreeB}}$ is not satisfied, since the solution is constrained to be periodic, which can cause large errors[7].

Simchony, Chellappa and Shao suggest in [49] a non-iterative way to solve the Poisson equation (21) using direct analytical methods (see Section 3.4). As observed by Lee in [37], the discretized Laplacian operator on a rectangular domain is a symmetric tridiagonal Toeplitz matrix if a Dirichlet boundary condition is used, whose eigenvalues are analytically known. Simchony, Chellappa and Shao show how to use the *discrete sine transform* to diagonalize such a matrix. They design an efficient solver for Eq. (21), which satisfies $\mathcal{P}_{\text{Fast}}$, $\mathcal{P}_{\text{Robust}}$ and $\mathcal{P}_{\text{NoPar}}$. Another extension of $\mathcal{M}_{\text{SCS}}$ to Neumann boundary conditions using the *discrete cosine transform* is suggested, which allows $\mathcal{P}_{\text{FreeB}}$ to be satisfied as well. Even if *embedding techniques* are supposed to generalize this method to non-rectangular domains, $\mathcal{P}_{\text{NoRect}}$ is not satisfied in practice. Neither is $\mathcal{P}_{\text{Disc}}$.

Horovitz and Kiryati improve $\mathcal{M}_{\text{HB}}$ in three ways [28,29]. They suggest how to ensure $\mathcal{P}_{\text{FreeB}}$. They also show how to incorporate the depth in some sparse *control points*, in order to correct a possible bias in the reconstruction. Finally, they design a coarse-to-fine multigrid computation, in order to satisfy $\mathcal{P}_{\text{Fast}}$[8]. This acceleration technique however requires a parameter to be tuned, which loses $\mathcal{P}_{\text{NoPar}}$.

As in [19], Petrovic et al. enforce integrability [45], but the normal field is directly handled under its discrete writing, in a Bayesian framework. Using the notations of Section 3.3, a *graphical model* is constructed. An iterative algorithm known as *belief propagation* is used to converge towards the MAP estimate of the unknown surface gradient. It is claimed that "discontinuities are maintained", but too few results are provided to decide whether $\mathcal{P}_{\text{Disc}}$ is really satisfied.

In [34], Kimmel and Yavneh show how to accelerate the multigrid method designed by Horovitz and Kiryati [28] in the case where "the surface height at specific coordinates or along a curve" is known, using an *algebraic multigrid* approach. Basically, their method has the same properties as [28], although $\mathcal{P}_{\text{Fast}}$ is even better satisfied.

An alternative derivation of Eq. (35) is yielded by Wei and Klette in [53], in which the preliminary derivation of the Euler-Lagrange equation (21) associated to $\mathcal{F}_{L_2}(z)$ is not needed. They claim that "to solve the minimization problem, we employ the Fourier transform theory rather than variational approach to avoid using the initial and boundary conditions", but since a periodic boundary condition is actually used instead, $\mathcal{P}_{\text{FreeB}}$ is not satisfied. They also add two regularization terms to the functional $\mathcal{F}_{L_2}(z)$ given in Eq. (19), "in order to improve the accuracy and robustness". The property $\mathcal{P}_{\text{NoPar}}$ is thus lost. On the other hand, even if Wei and Klette note that "[$\mathcal{M}_{\text{HB}}$] is very sensitive to abrupt changes in orientation, i.e., there are large errors at the object boundary", their method does not satisfy $\mathcal{P}_{\text{Disc}}$ either, whereas we will observe that loosing $\mathcal{P}_{\text{NoPar}}$ is often the price to satisfy $\mathcal{P}_{\text{Disc}}$.

Another method inspired by $\mathcal{M}_{\text{FC}}$ is that of Kovesi [36]. Instead of projecting the given gradient field on a Fourier basis, Kovesi suggests to compute the correlations of this gradient field with the gradient fields of a *bank of shapelets*, which are in practice a family of Gaussian surfaces[9]. This method globally satisfies the same properties as $\mathcal{M}_{\text{FC}}$ but, in addition, it can be applied to an *incomplete normal field* i.e., to normals whose tilts are known up to a certain ambiguity[10]. Although photometric stereo computes the normals without ambiguity, this peculiarity could indeed be useful when a couple of images only is used, or *a fortiori* a single image (shape-from-shading), since the problem is not well-posed in both these cases.

In [26], Ho, Lim, Yang and Kriegman derive from Eq. (4) the *eikonal equation* $\|\nabla z\|^2 = p^2+q^2$ (under the

[7] Noakes, Kozera and Klette follow the same way as Frankot and Chellappa but, since they use a set $\mathcal{I}$ of integrable vector fields which is not spanned by the Fourier basis, they cannot resort to the very efficient Fast Fourier Transform algorithm any more [41,43].

[8] Goldman et al. do the same using the conjugate gradient method [21].

[9] According to [2], Kovesi uses "a redundant set of non-orthogonal basis functions".

[10] http://www.peterkovesi.com/matlabfns/index.html#shapelet

assumption $\mathsf{m} = 1$), and aspire to use the *fast marching* method for its resolution. Unfortunately, this method requires that the unknown z has a unique global minimum over Ω. Thereby, a more general eikonal equation $\|\nabla(z + \lambda f)\|^2 = (p + \lambda \partial_u f)^2 + (q + \lambda \partial_v f)^2$ is solved, where f is a known function and the parameter λ has to be tuned so that $z + \lambda f$ has a unique global minimum. The main advantage is that $\mathcal{P}_{\text{Fast}}$ is (widely) satisfied. Nothing is said about robustness, but we guess that error accumulation occurs as the depth is computed from the global minimum, level set by level set.

As already explained in Section 3.2, Durou and Courteille improve $\mathcal{M}_{\text{HB}}$ in [16], in order to satisfy $\mathcal{P}_{\text{FreeB}}$[11]. A very similar improvement of $\mathcal{M}_{\text{HB}}$ is proposed by Harker and O'Leary in [22]. The latter loses the ability to handle any domain of integration, whereas the reformulation of the problem as a *Sylvester equation* provides two appreciable improvements. First, it deals with matrices of the same size as the initial (regular) grid and resorts to very efficient solvers dedicated to Sylvester equations, thus satisfying $\mathcal{P}_{\text{Fast}}$. Moreover, any form of discrete derivatives is allowed. In [23,24], Harker and O'Leary moreover propose several variants including regularization, which are still written as Sylvester equations, but one of them loses the property $\mathcal{P}_{\text{FreeB}}$, whereas the others lose $\mathcal{P}_{\text{NoPar}}$.

In [17], Ettl et al. propose a method specifically designed for *deflectometry*, which aims at measuring "height variations as small as a few nanometers" and delivers normal fields "with small noise and curl", but the normals are provided on an *irregular grid*. This is why Ettl et al. search for an interpolating/approximating surface rather than for one unknown value per sample. Of course, this method is highly parametric, but $\mathcal{P}_{\text{NoPar}}$ is still satisfied, since the parameters are the unknowns. Its main problem is that $\mathcal{P}_{\text{Fast}}$ is rarely satisfied, depending on the number of parameters that are used.

The fast-marching method [26] is improved in [20] by Galliani, Breuss and Ju in three ways. First, the method by Ho et al. is shown to be inaccurate, due to the use of analytical derivatives $\partial_u f$ and $\partial_v f$ in the eikonal equation, instead of discrete derivatives. An *upwind scheme* is more appropriate to solve such a PDE. Second, the new method is more stable and the choice of λ is no more a cause for concern. This implies that $\mathcal{P}_{\text{NoPar}}$ is satisfied *de facto*. Finally, any form of domain Ω can be handled, but it is not clear whether $\mathcal{P}_{\text{NoRect}}$ was not satisfied by the former method yet. Not surprisingly, this new method is not robust, even its if robustness is improved in a more recent paper [6], but it can be used as initialization for more robust methods based, for instance, on quadratic regularization [10].

The integration method proposed by Balzer in [8] is based on second order shape derivatives, allowing for the use of a fast Gauss-Newton algorithm. Hence $\mathcal{P}_{\text{Fast}}$ is satisfied. A careful meshing of the problem, as well as the use of a finite element method, make $\mathcal{P}_{\text{NoRect}}$ to be satisfied. However, for the very same reason, $\mathcal{P}_{\text{NoPar}}$ is not satisfied. Moreover, the method is limited to smooth surfaces, and therefore $\mathcal{P}_{\text{Disc}}$ cannot be satisfied. Finally, $\mathcal{P}_{\text{Robust}}$ can be achieved thanks to a premiminary filtering step. Balzer and Mörwald design in [9] another finite element method, where the surface model is based on *B-splines*. It satisfies the same properties as the previous method[12].

In [58], Xie et al. deform a mesh "to let its facets follow the demanded normal vectors", resorting to discrete geometry processing. As a non-parametric surface model is used, $\mathcal{P}_{\text{FreeB}}$, $\mathcal{P}_{\text{NoPar}}$ and $\mathcal{P}_{\text{NoRect}}$ are satisfied. In order to avoid the oversmoothing effect of many previous methods, sharp features can be preserved. However, $\mathcal{P}_{\text{Disc}}$ is not addressed. On the other hand, $\mathcal{P}_{\text{Fast}}$ is not satisfied since the proposed method alternates local and global optimization.

In [59], Yamaura et al. design a new method based on B-splines, which has the same properties as that proposed in [9]. But since the latter "relies on second-order partial differential equations, which is inefficient and unnecessary, as normal vectors consist of only first-order derivatives", a simpler formalism with higher performances is proposed. Moreover, a nice application to surface editing is exhibited.

4.3.2 Methods which care about Discontinuities

The first work which *really* addresses the problem of $\mathcal{P}_{\text{Disc}}$ is by Karaçali and Snyder [32,33], who show how to define a new orthonormal basis of integrable vector fields which can incorporate depth discontinuities. They moreover show how to detect such discontinuities, in order to *partially* enforce integrability. The designed method thus satisfies $\mathcal{P}_{\text{Disc}}$, as well as $\mathcal{P}_{\text{Robust}}$ and $\mathcal{P}_{\text{FreeB}}$, but $\mathcal{P}_{\text{Fast}}$ is lost, despite the use of a block processing technique inspired by the work of Noakes et al. [41,43]. In accordance with a previous remark, since it is often the price to satisfy $\mathcal{P}_{\text{Disc}}$, $\mathcal{P}_{\text{NoPar}}$ is also lost.

In [1], Agrawal, Chellappa and Raskar consider the pixels as a weighted graph, such that the weights are of the form $p_{u,v+1} - p_{u,v} - q_{u+1,v} + q_{u,v}$. Each edge whose weight is greater than a threshold is cut. A minimal

[11] A preliminary version of this method was already described in [13].

[12] https://github.com/jonabalzer/iga-integration/tree/master/core

number of suppressed edges are then restored, in order to reconnect the graph while minimizing the total weight. As soon as an edge is still missing, one gradient value $p_{u,v}$ or $q_{u,v}$ is considered as possibly corrupted. It is shown how these suspected gradient values can be corrected, in order to enforce integrability "with the important property of local error confinement". Neither $\mathcal{P}_{\text{FreeB}}$ nor $\mathcal{P}_{\text{NoPar}}$ is satisfied, and $\mathcal{P}_{\text{Fast}}$ is not guaranteed as well, even if the method is non-iterative. Moreover, the following is asserted in [46]: "Under noise, the algorithm in [1] confuses correct gradients as outliers and performs poorly". Finally, $\mathcal{P}_{\text{Disc}}$ may be satisfied since strict integrability is no more uniformly imposed over the entire gradient field.

In [2], Agrawal, Raskar and Chellappa propose a general framework "based on controlling the anisotropy of weights for gradients during the integration"[13]. They are much inspired by classical image restoration techniques. It is shown how the (isotropic) Laplacian operator in Eq. (21) must be modified using "spatially varying anisotropic kernels", thus obtaining four methods: two based on robust estimation, one on regularization, and one on anisotropic diffusion[14]. A homogeneous Neumann boundary condition $\nabla z \cdot \boldsymbol{\eta} = 0$ is assumed, which looks rather unrealistic. Thus, the four proposed methods do not satisfy $\mathcal{P}_{\text{FreeB}}$, neither $\mathcal{P}_{\text{Fast}}$ nor $\mathcal{P}_{\text{NoPar}}$. Nevertheless, a special attention is given to satisfy $\mathcal{P}_{\text{Robust}}$ and $\mathcal{P}_{\text{Disc}}$.

A similar method to the first one proposed in [2] is designed by Fraile and Hancock in [18]. A *minimum spanning tree* is constructed from the same graph of pixels as in [1], except that the weights are different (several weights are tested). The integral of Eq. (6) along the unique path joining each pixel to a root pixel is then computed. Of course, this method is less robust than those based on quadratic regularization (or than the weighted quadratic regularization proposed in [2]), since "the error due to measurement noise propagates along the path", and it is rather slow because of the search for a minimum spanning tree. But, depending on which weights are used, it could preserve depth discontinuities: in such a case as that of Fig. 3-a, each pixel could be reached from a root pixel without crossing any discontinuity.

In [56], Wu and Tang try to find the best compromise between integrability and discontinuity preservation. In order to segment the scene into pieces without discontinuities, "one plausible method [...] is to identify where the integrability constraint is violated", but "in real case, [this] may produce very poor discontinuity maps rendering them unusable at all". A probabilistic method using the EM (Expectation-Maximization) algorithm is thus proposed, which provides a weighted discontinuity map. The alternating iterative optimization is very slow and a parameter is used, but this approach is promising, even if the evaluation of the results remains qualitative.

In [39,40], Ng, Wu and Tang do not enforce integrability over the entire domain, because with such an enforcement "sharp features will be smoothed out and surface distortion will be produced". Since "either sparse or dense, residing on a 2D regular (image) or irregular grid space" gradient fields may be integrated, it is concluded that "a continuous formulation for surface-from-gradients is preferred". Gaussian *kernel functions* are used, in order to linearize the problem and to avoid the need for extra knowledge on the boundary[15]. Unfortunately, at least two parameters must be tuned. Also $\mathcal{P}_{\text{Fast}}$ is not satisfied, not more than $\mathcal{P}_{\text{FreeB}}$, as shown in [9] on the basis of several examples. On the other hand, the proposed method outputs "continuous 3D representation not limited to a height field".

In [46], Reddy, Agrawal and Chellappa propose a method specifically designed to handle heavily corrupted gradient fields, which combines "the best of least squares and combinatorial search to handle noise and correct outliers respectively". Even it is claimed that "L_1 solution performs well across all scenarios without the need for any tunable parameter adjustments", $\mathcal{P}_{\text{NoPar}}$ is not satisfied in practice. Neither is $\mathcal{P}_{\text{FreeB}}$.

In [15], Durou, Aujol and Courteille are mainly concerned by $\mathcal{P}_{\text{Disc}}$. Knowing that quadratic regularization works well in the case of smooth surfaces, but is not well adapted to discontinuities, the use of other regularizers, or of other variational models inspired by image processing, as in [2], allows $\mathcal{P}_{\text{Disc}}$ to be satisfied. This will be detailed in our second paper.

The integration method proposed in [47,48] by Saracchini, Stolfi, Leitão, Atkinson and Smith[16] is a multi-scale version of $\mathcal{M}_{\text{HB}}$. A system is solved at each scale using a Gauss-Seidel iteration in order to satisfy $\mathcal{P}_{\text{Fast}}$. Since reliability in the gradient is used as local weight, "each equation can be tuned to ignore bad data samples and suspected discontinuities", thus allowing $\mathcal{P}_{\text{Disc}}$ to be satisfied. Finally, setting the weights outside Ω to zero allows $\mathcal{P}_{\text{FreeB}}$ and $\mathcal{P}_{\text{NoRect}}$ to be satisfied as well. However, this method "assumes that the slope and weight maps are given". But such a weight map is a crucial clue, and the following assertion somehow

[13] http://www.amitkagrawal.com/eccv06/RangeofSurfaceReconstructions.html

[14] A similar approach will be detailed in our second paper.

[15] http://www.cse.ust.hk/~pang/papers/supp_materials/pami_sur3d_code.zip

[16] http://www.ic.unicamp.br/stolfi/EXPORT/projects/photo-stereo/

avoids the problem: "practical integration algorithms require the user to provide a weight map".

A similar approach is followed by Wang, Bu, Li, Song and Tan in [52], but the weight map is *binary* and automatically computed. In addition to the gradient map, the photometric stereo images themselves are required. Eight cues are used by two SVM classifiers, which have to be trained using synthetic labelled data. Even if the results are nice, the proposed method seems rather difficult to manage in practice, and clearly loses $\mathcal{P}_{\text{Fast}}$ and $\mathcal{P}_{\text{NoPar}}$.

In [4,5], Badri, Yahia and Aboutajdine resort to L_p norms, $p \in]0,1[$. As p decreases, the L_0 norm is approximated, which is a sparse estimator well adapted to outliers. Indeed, the combination of four terms allows Badri et al. to design a method which simultaneously handles noise and outliers, thus ensuring that $\mathcal{P}_{\text{Robust}}$ and $\mathcal{P}_{\text{Disc}}$ are satisfied. However, since the problem becomes non-convex, the proposed *half-quad* resolution is iterative and requires a good initialization: $\mathcal{P}_{\text{Fast}}$ is lost. It happens that neither $\mathcal{P}_{\text{NoPar}}$ is satisfied. Finally, even if each iteration resorts to FFT, which implies a rectangular domain and a periodic boundary condition, the proposed scheme seems easily extendable so as to satisfy $\mathcal{P}_{\text{FreeB}}$ and $\mathcal{P}_{\text{NoRect}}$.

4.4 Summary of the Review

Our discussion on the most representative methods of integration is summarized in Table 1, where the methods are listed in chronological order. It appears that none of them satisfies all the required properties, which is not surprising. On the other hand, even if accuracy is the most basic property of any 3D-reconstruction technique, let us recall that it would have been impossible in practice to numerically compare all these methods.

In view of Table 1, it appears that almost every method differs from all the others, regarding the six selected properties. Of course, it may appear that such a binary (+/−) table is hardly informative, but more levels in each criterion would have led to more arbitrary scores. On the other hand, the number of + should not be considered as a global score for a given method: it happens that a method perfectly satisfies a subset of properties, while it does not care at all about the others.

5 Conclusion and Perspectives

Even if robustness to outliers was not selected in our list of required properties, let us cite a paper specifically dedicated to this problem. In [14], Du, Robles-Kelly and Lu compare the L_2 and L_1 norms, as well as a number of M-estimators, faced to the presence of outliers in the normal field: L_1 is shown to be the globally best parry. This paper being worthwhile, one can wonder why it does not appear in Table 1. On the one hand, even if $\mathcal{P}_{\text{Robust}}$ is satisfied at best, none of the other criteria are considered. On the other hand, let us recall why we did not select robustness to outliers as a pertinent feature: the presence of outliers in the normal field does not have to be compensated by the integration method. In [5], it is said that "[photometric stereo] can fail due to the presence of shadows and noise", but recall that photometric stereo can be robust to outliers [30,55].

Another property was ignored: whether the depth can be fixed at some points or not. As integration is a well-posed problem without any additional knowledge on the solution, we considered that this property is appreciable, although not required. Let us however quote, once again, the papers by Horovitz and Kiryati [29] and by Kimmel and Yavneh [34], in which this problem is specifically dealt with.

Some other works on normal integration have not been mentioned in our review, since they address other problems or do not face the same challenges. Let us first cite a work by Balzer [7], in which a specific problem with the normals delivered by deflectometry is highlighted: as noted by Ettl et al. in [17], such normals are usually not noisy, but Balzer points out that they are *distant-dependent*, which means that the gradient field $\mathbf{g} = [p, q]^\top$ also depends on the depth z. The iterative method proposed in [7] to solve this more general problem seems to be quite limited, but an interesting extension to normals provided by photometric stereo is suggested: "one could abandon the widespread assumption that the light sources are distant and the lighting directions thus constant".

On the other hand, Chang et al. address in [11] the problem of *multiview normal integration*, which aims at reconstructing a full 3D-shape in the framework of multiview photometric stereo. The original variational formulation (19) is extended to such normal fields, and the resulting PDE is solved via a level set method, which has to be soundly initialized. The 3D-reconstructions are nice but are limited to synthetic multiview photometric stereo images. However, this approach should be continued, since it provides complete 3D-models. Moreover, it is noted in [11] that the use of multiview inputs is the most intuitive way to satisfy $\mathcal{P}_{\text{Disc}}$.

As noticed by Agrawal et al. about the range of solutions proposed in [2], but this is more generally true, "the choice of using a particular algorithm for a given application remains an open problem". We hope this review will help the reader to make up its own mind, faced to so many existing approaches.

Table 1 Main methods of integration listed in chronological order.

Authors	Year	Ref.	$\mathcal{P}_{\text{Fast}}$	$\mathcal{P}_{\text{Robust}}$	$\mathcal{P}_{\text{FreeB}}$	$\mathcal{P}_{\text{Disc}}$	$\mathcal{P}_{\text{NoPar}}$	$\mathcal{P}_{\text{NoRect}}$
Coleman and Jain	1982	[12]	+	−	+	−	+	+
Horn and Brooks	1986	[27]	−	+	−	−	+	+
Frankot and Chellappa	1988	[19]	+	+	−	−	+	−
Simchony, Chellappa and Shao	1990	[49]	+	+	+	−	+	−
Noakes, Kozera and Klette	1999	[43]	−	+	−	−	+	−
Horovitz and Kiryati	2000	[28]	+	+	+	−	−	+
Petrovic et al.	2001	[45]	−	+	+	−	−	+
Kimmel and Yavneh	2003	[34]	+	+	+	−	−	+
Wei and Klette	2003	[53]	+	+	−	−	−	−
Karaçali and Snyder	2003	[32]	−	+	+	+	−	−
Kovesi	2005	[36]	+	+	−	−	+	−
Agrawal, Chellappa and Raskar	2005	[1]	−	−	−	+	−	+
Agrawal, Raskar and Chellappa	2006	[2]	−	+	−	+	−	+
Fraile and Hancock	2006	[18]	−	−	+	+	+	+
Ho, Lim, Yang and Kriegman	2006	[26]	+	−	+	−	−	+
Wu and Tang	2006	[56]	−	+	+	+	−	+
Ng, Wu and Tang	2007	[39]	−	+	−	+	−	+
Durou and Courteille	2007	[16]	−	+	+	−	+	+
Harker and O'Leary	2008	[22]	+	+	+	−	+	−
Ettl, Kaminski, Knauer and Häusler	2008	[17]	−	+	+	−	+	+
Reddy, Agrawal and Chellappa	2009	[46]	−	+	−	+	−	+
Durou, Aujol and Courteille	2009	[15]	−	+	+	+	−	+
Saracchini et al.	2010	[47]	+	+	+	+	−	+
Galliani, Breuss and Ju	2012	[20]	+	−	+	−	+	+
Balzer	2012	[8]	+	+	+	−	−	+
Wang, Bu, Li, Song and Tan	2012	[52]	−	+	+	+	−	+
Balzer and Mörwald	2012	[9]	+	+	+	−	−	+
Xie, Zhang, Wang and Chung	2014	[58]	−	+	+	−	+	+
Badri, Yahia and Aboutajdine	2014	[5]	−	+	+	+	−	+
Yamaura, Nanya, Imoto and Maekawa	2015	[59]	+	+	+	−	−	+
Breuss, Quéau, Bähr and Durou	2016	[10]	+	+	+	−	+	+

Finally, even if none of the reviewed methods satisfies all the selected criteria, this work helped us to develop some new normal integration methods. In the second part of our work, entitled *Part II: New Insights*, we will particularly focus on the problem of normal integration in the presence of discontinuities, which occurs as soon as there are occlusions.

References

1. Agrawal, A., Chellappa, R., Raskar, R.: An Algebraic Approach to Surface Reconstruction from Gradient Fields. In: Proceedings of the 10$^{\text{th}}$ IEEE International Conference on Computer Vision (volume I), pp. 174–181. Beijing, China (2005) 13, 14, 16
2. Agrawal, A., Raskar, R., Chellappa, R.: What Is the Range of Surface Reconstructions from a Gradient Field? In: Proceedings of the 9$^{\text{th}}$ European Conference on Computer Vision (volume I), *Lecture Notes in Computer Science*, vol. 3951, pp. 578–591. Graz, Austria (2006) 7, 12, 14, 15, 16
3. Aubert, G., Aujol, J.F.: Poisson skeleton. Tech. rep., Laboratoire Jean Alexandre Dieudonné - JAD, Institut de Mathématiques de Bordeaux - IMB (2012) 4
4. Badri, H., Yahia, H.: A Non-Local Low-Rank Approach to Enforce Integrability. IEEE Transactions on Image Processing (2016) 15
5. Badri, H., Yahia, H., Aboutajdine, D.: Robust Surface Reconstruction via Triple Sparsity. In: Proceedings of the IEEE Conference on Computer Vision and Pattern Recognition. Columbus, Ohio, USA (2014) 15, 16
6. Bähr, M., Breuss, M.: An Improved Eikonal Equation for Surface Normal Integration. In: Proceedings of the 37$^{\text{th}}$ German Conference on Pattern Recognition. Aachen, Germany (2015) 13
7. Balzer, J.: Shape from Specular Reflection in Calibrated Environments and the Integration of Spatial Normal Fields. In: Proceedings of the 18$^{\text{th}}$ IEEE International Conference on Image Processing, pp. 21–24. Brussels, Belgium (2011) 15
8. Balzer, J.: A Gauss-Newton Method for the Integration of Spatial Normal Fields in Shape Space. Journal of Mathematical Imaging and Vision **44**(1), 65–79 (2012) 13, 16
9. Balzer, J., Mörwald, T.: Isogeometric Finite-Elements Methods and Variational Reconstruction Tasks in Vision - A Perfect Match. In: Proceedings of the IEEE Conference on Computer Vision and Pattern Recognition. Providence, Rhode Island, USA (2012) 13, 14, 16
10. Breuss, M., Quéau, Y., Bähr, M., Durou, J.D.: Fast and Accurate Surface Normal Integration on Non-Rectangular Domains. Computational Visual Media (to appear in 2017) 13, 16
11. Chang, J.Y., Lee, K.M., Lee, S.U.: Multiview Normal Field Integration Using Level Set Methods. In: Proceedings of the IEEE Conference on Computer Vision and Pattern Recognition, Workshop on Beyond Multiview Geometry: Robust Estimation and Organization

of Shapes from Multiple Cues. Minneapolis, Minnesota, USA (2007) 15
12. Coleman, E.N., Jain, R.: Obtaining 3-Dimensional Shape of Textured and Specular Surfaces Using Four-Source Photometry. Computer Graphics and Image Processing **18**(4), 309–328 (1982) 4, 11, 16
13. Crouzil, A., Descombes, X., Durou, J.D.: A Multiresolution Approach for Shape from Shading Coupling Deterministic and Stochastic Optimization. IEEE Transactions on Pattern Analysis and Machine Intelligence **25**(11), 1416–1421 (2003) 13
14. Du, Z., Robles-Kelly, A., Lu, F.: Robust Surface Reconstruction from Gradient Field Using the L1 Norm. In: Proceedings of the 9th Biennial Conference of the Australian Pattern Recognition Society on Digital Image Computing Techniques and Applications, pp. 203–209. Glenelg, Australia (2007) 15
15. Durou, J.D., Aujol, J.F., Courteille, F.: Integration of a Normal Field in the Presence of Discontinuities. In: Proceedings of the 7th International Workshop on Energy Minimization Methods in Computer Vision and Pattern Recognition, *Lecture Notes in Computer Science*, vol. 5681, pp. 261–273. Bonn, Germany (2009) 14, 16
16. Durou, J.D., Courteille, F.: Integration of a Normal Field without Boundary Condition. In: Proceedings of the 11th IEEE International Conference on Computer Vision, 1st Workshop on Photometric Analysis for Computer Vision. Rio de Janeiro, Brazil (2007) 2, 5, 13, 16
17. Ettl, S., Kaminski, J., Knauer, M.C., Häusler, G.: Shape Reconstruction from Gradient Data. Applied Optics **47**(12), 2091–2097 (2008) 13, 15, 16
18. Fraile, R., Hancock, E.R.: Combinatorial Surface Integration. In: Proceedings of the 18th International Conference on Pattern Recognition (volume I), pp. 59–62. Hong Kong (2006) 14, 16
19. Frankot, R.T., Chellappa, R.: A Method for Enforcing Integrability in Shape from Shading Algorithms. IEEE Transactions on Pattern Analysis and Machine Intelligence **10**(4), 439–451 (1988) 1, 7, 8, 11, 12, 16
20. Galliani, S., Breuss, M., Ju, Y.C.: Fast and Robust Surface Normal Integration by a Discrete Eikonal Equation. In: Proceedings of the 23rd British Machine Vision Conference. Guildford, UK (2012) 13, 16
21. Goldman, D.B., Curless, B., Hertzmann, A., Seitz, S.M.: Shape and Spatially-Varying BRDFs From Photometric Stereo. In: Proceedings of the 10th IEEE International Conference on Computer Vision (volume I). Beijing, China (2005) 12
22. Harker, M., O'Leary, P.: Least Squares Surface Reconstruction from Measured Gradient Fields. In: Proceedings of the IEEE Conference on Computer Vision and Pattern Recognition. Anchorage, Alaska, USA (2008) 7, 13, 16
23. Harker, M., O'Leary, P.: Least Squares Surface Reconstruction from Gradients: Direct Algebraic Methods with Spectral, Tikhonov, and Constrained Regularization. In: Proceedings of the IEEE Conference on Computer Vision and Pattern Recognition. Colorado Springs, Colorado, USA (2011) 13
24. Harker, M., O'Leary, P.: Regularized Reconstruction of a Surface from its Measured Gradient Field. Journal of Mathematical Imaging and Vision **51**(1), 46–70 (2015) 5, 13
25. Healey, G., Jain, R.: Depth Recovery from Surface Normals. In: Proceedings of the 7th International Conference on Pattern Recognition, pp. 894–896. Montreal, Canada (1984) 4, 11
26. Ho, J., Lim, J., Yang, M.H.: Integrating Surface Normal Vectors Using Fast Marching Method. In: Proceedings of the 9th European Conference on Computer Vision (volume III), *Lecture Notes in Computer Science*, vol. 3953, pp. 239–250. Graz, Austria (2006) 12, 13, 16
27. Horn, B.K.P., Brooks, M.J.: The Variational Approach to Shape From Shading. Computer Vision, Graphics, and Image Processing **33**(2), 174–208 (1986) 1, 4, 5, 11, 16
28. Horovitz, I., Kiryati, N.: Bias Correction in Photometric Stereo Using Control Points. Tech. rep., Department of Electrical Engineering Systems, Tel Aviv University, Israel (2000) 12, 16
29. Horovitz, I., Kiryati, N.: Depth from Gradient Fields and Control Points: Bias Correction in Photometric Stereo. Image and Vision Computing **22**(9), 681–694 (2004) 3, 11, 12, 15
30. Ikehata, S., Wipf, D., Matsushita, Y., Aizawa, K.: Photometric Stereo Using Sparse Bayesian Regression for General Diffuse Surfaces. IEEE Transactions on Pattern Analysis and Machine Intelligence **36**(9), 1816–1831 (2014) 15
31. Ikeuchi, K.: Constructing A Depth Map from Images. Technical Memo AIM-744, Artificial Intelligence Laboratory, Massachusetts Institute of Technology, Cambridge, Massachusetts, USA (1983) 11
32. Karaçali, B., Snyder, W.: Reconstructing Discontinuous Surfaces from a Given Gradient Field using Partial Integrability. Computer Vision and Image Understanding **92**(1), 78–111 (2003) 13, 16
33. Karaçali, B., Snyder, W.: Noise Reduction in Surface Reconstruction from a Given Gradient Field. International Journal of Computer Vision **60**(1), 25–44 (2004) 13
34. Kimmel, R., Yavneh, I.: An Algebraic Multigrid Approach for Image Analysis. SIAM Journal on Scientific Computing **24**(4), 1218–1231 (2003) 12, 15, 16
35. Klette, R., Schlüns, K.: Height Data from Gradient Fields. In: Proceedings of the Machine Vision Applications, Architectures, and Systems Integration, *Proceedings of the International Society for Optical Engineering*, vol. 2908, pp. 204–215. Boston, Massachusetts, USA (1996) 6, 11
36. Kovesi, P.: Shapelets Correlated with Surface Normals Produce Surfaces. In: Proceedings of the 10th IEEE International Conference on Computer Vision (volume II), pp. 994–1001. Beijing, China (2005) 12, 16
37. Lee, D.: A Provably Convergent Algorithm for Shape from Shading. In: Proceedings of the DARPA Image Understanding Workshop, pp. 489–496. Miami Beach, Florida, USA (1985) 12
38. Miranda, C.: Partial differential equations of elliptic type, second edn. Springer-Verlag (1970) 4
39. Ng, H.S., Wu, T.P., Tang, C.K.: Surface-from-Gradients with incomplete data for single view modeling. In: Proceedings of the 11th IEEE International Conference on Computer Vision. Rio de Janeiro, Brazil (2007) 7, 14, 16
40. Ng, H.S., Wu, T.P., Tang, C.K.: Surface-from-Gradients without Discrete Integrability Enforcement: A Gaussian Kernel Approach. IEEE Transactions on Pattern Analysis and Machine Intelligence **32**(11), 2085–2099 (2010) 11, 14
41. Noakes, L., Kozera, R.: The 2-D Leap-Frog: Integrability, Noise, and Digitization. In: G. Bertrand, A. Imiya, R. Klette (eds.) Digital and Image Geometry, *Lecture Notes in Computer Science*, vol. 2243, pp. 352–364. Springer-Verlag (2001) 12, 13
42. Noakes, L., Kozera, R.: Nonlinearities and Noise Reduction in 3-Source Photometric Stereo. Journal of Mathematical Imaging and Vision **18**(2), 119–127 (2003) 10

43. Noakes, L., Kozera, R., Klette, R.: The Lawn-Mowing Algorithm for Noisy Gradient Vector Fields. In: Vision Geometry VIII, *Proceedings of the International Society for Optical Engineering*, vol. 3811, pp. 305–316. Denver, Colorado, USA (1999) 12, 13, 16
44. Pérez, P., Gangnet, M., Blake, A.: Poisson image editing. ACM Transactions on Graphics **22**(3), 313–318 (2003) 4
45. Petrovic, N., Cohen, I., Frey, B.J., Koetter, R., Huang, T.S.: Enforcing Integrability for Surface Reconstruction Algorithms Using Belief Propagation in Graphical Models. In: Proceedings of the IEEE Conference on Computer Vision and Pattern Recognition (volume I), pp. 743–748. Kauai, Hawaii, USA (2001) 12, 16
46. Reddy, D., Agrawal, A., Chellappa, R.: Enforcing Integrability by Error Correction using l1-minimization. In: Proceedings of the IEEE Conference on Computer Vision and Pattern Recognition. Miami, Florida, USA (2009) 11, 14, 16
47. Saracchini, R.F.V., Stolfi, J., Leitão, H.C.G., Atkinson, G.A., Smith, M.L.: Multi-Scale Depth from Slope with Weights. In: Proceedings of the 21st British Machine Vision Conference. Aberystwyth, UK (2010) 14, 16
48. Saracchini, R.F.V., Stolfi, J., Leitão, H.C.G., Atkinson, G.A., Smith, M.L.: A Robust Multi-Scale Integration Method to Obtain the Depth From Gradient Maps. Computer Vision and Image Understanding **116**(8), 882–895 (2012) 7, 11, 14
49. Simchony, T., Chellappa, R., Shao, M.: Direct Analytical Methods for Solving Poisson Equations in Computer Vision Problems. IEEE Transactions on Pattern Analysis and Machine Intelligence **12**(5), 435–446 (1990) 4, 7, 9, 10, 12, 16
50. Stoer, J., Burlirsch, R.: Introduction to Numerical Analysis. Text in Applied Mathematics. Springer (2002) 5
51. Tankus, A., Kiryati, N.: Photometric Stereo under Perspective Projection. In: Proceedings of the 10th IEEE International Conference on Computer Vision (volume I), pp. 611–616. Beijing, China (2005) 3
52. Wang, Y., Bu, J., Li, N., Song, M., Tan, P.: Detecting Discontinuities for Surface Reconstruction. In: Proceedings of the 21st International Conference on Pattern Recognition, pp. 2108–2111. Tsukuba, Japan (2012) 14, 16
53. Wei, T., Klette, R.: Depth Recovery from Noisy Gradient Vector Fields Using Regularization. In: Proceedings of the 10th International Conference on Computer Analysis of Images and Patterns, *Lecture Notes in Computer Science*, vol. 2756, pp. 116–123. Groningen, The Netherlands (2003) 12, 16
54. Woodham, R.J.: Photometric Method for Determining Surface Orientation from Multiple Images. Optical Engineering **19**(1), 139–144 (1980) 7
55. Wu, L., Ganesh, A., Shi, B., Matsushita, Y., Wang, Y., Ma, Y.: Robust Photometric Stereo via Low-Rank Matrix Completion and Recovery. In: Proceedings of the 10th Asian Conference on Computer Vision, pp. 703–717. Queenstown, New Zealand (2010) 15
56. Wu, T.P., Tang, C.K.: Visible Surface Reconstruction from Normals with Discontinuity Consideration. In: Proceedings of the IEEE Conference on Computer Vision and Pattern Recognition (volume II), pp. 1793–1800. New York, USA (2006) 14, 16
57. Wu, Z., Li, L.: A Line-Integration Based Method for Depth Recovery from Surface Normals. Computer Vision, Graphics, and Image Processing **43**(1), 53–66 (1988) 4, 11
58. Xie, W., Zhang, Y., Wang, C.C.L., Chung, R.C.K.: Surface-from-Gradients: An Approach Based on Discrete Geometry Processing. In: Proceedings of the IEEE Conference on Computer Vision and Pattern Recognition. Columbus, Ohio, USA (2014) 13, 16
59. Yamaura, Y., Nanya, T., Imoto, H., Maekawa, T.: Shape reconstruction from a normal map in terms of uniform bi-quadratic B-spline surfaces. Computer-Aided Design **63**, 129–140 (2015) 13, 16
60. Yuille, A.L., Snow, D.: Shape and Albedo from Multiple Images using Integrability. In: Proceedings of the IEEE Conference on Computer Vision and Pattern Recognition, pp. 158–164. San Juan, Puerto Rico (1997) 11